

---

# Regional evaluation of hydraulic properties in variably fractured rock using a hydrostructural domain approach

M. Surrrette · D. M. Allen · M. Journeay

**Abstract** A hydrostructural domain approach was tested and validated in fractured bedrock aquifers of the Gulf Islands, British Columbia (BC), Canada. Relative potential hydraulic properties for three hydrostructural domains in folded and faulted sedimentary rocks were derived using stochastically generated fracture data and hybrid discrete fracture network-equivalent porous media (DFN-EPM) modelling. Model-derived relative potential transmissivity values show good spatial agreement with transmissivity values obtained from pumping tests at selected sites. A spatial pattern of increasing transmissivity towards the southeast along the island chain is consistent between both datasets. Cluster analysis on relative potential permeability values obtained from a larger dataset for the region identified four clusters with geometric means of  $9 \times 10^{-13}$ ,  $4 \times 10^{-13}$ ,  $2 \times 10^{-13}$ , and  $3 \times 10^{-14}$  m<sup>2</sup>. The general trend is an increase in relative potential permeability toward the southeast, emulating the trends identified in the site-specific analyses. Relative potential permeability values increase with proximity to the hinge line of a regional northwest-trending asymmetric fault propagation fold structure, and with proximity to superimposed high-angle north- and northeast-trending brittle faults. The results are consistent with documented patterns of structurally controlled fluid flow and show

promise for use in regional characterization of fractured bedrock aquifers.

**Résumé** Une approche par domaine structural a été testée et validée dans des aquifères de socle fracturé des îles du Golfe en Colombie Britannique (CB) au Canada. Les propriétés hydrauliques relatives potentielles, de trois domaines structuraux dans des roches sédimentaires plissées et faillées, ont été dérivées en utilisant des données de fractures générées de façon stochastique et la modélisation hybride couplant les approches milieu poreux équivalent et réseau de fractures discrètes (DFN-EPM en anglais). Les valeurs de transmissivités relatives potentielles dérivées du modèle montrent une bonne concordance spatiale avec les valeurs de transmissivité calculées à partir d'essais de pompage pour des sites sélectionnés. Une tendance spatiale de la valeur de transmissivité à l'augmentation en direction du sud-ouest le long de la chaîne d'îles est cohérent entre les deux jeux de données. Quatre familles avec les moyennes géométriques de  $9 \times 10^{-13}$ ,  $4 \times 10^{-13}$ ,  $2 \times 10^{-13}$ , et  $3 \times 10^{-14}$  m<sup>2</sup> ont été identifiées grâce à une analyse de regroupement sur des valeurs de perméabilité relatives potentielles issues d'un jeu de données régionales plus large. La tendance générale est une augmentation de la perméabilité relative potentielle en direction du sud-ouest, ce qui coïncide avec les tendances identifiées dans les études spécifiques au site. Les valeurs de perméabilité relatives potentielles augmentent en fonction de la distance à la charnière d'une structure en pli de propagation d'une faille asymétrique régionale à tendance nord-ouest, et en fonction de la distance à des failles cassantes superposées, à angle fort et à tendance nord/nord-ouest. Les résultats sont cohérents avec les tendances rapportées d'écoulement de fluide contrôlé par la structure et sont prometteurs pour la caractérisation régionale des aquifères de socle fracturé.

---

Received: 29 January 2007 / Accepted: 22 June 2007  
Published online: 3 September 2007

© Springer-Verlag 2007

---

**Electronic supplementary material** The online version of this article (doi:10.1007/s10040-007-0206-9) contains supplementary material, which is available to authorized users.

---

M. Surrrette · D. M. Allen (✉)  
Department of Earth Sciences,  
Simon Fraser University,  
Burnaby, BC V5A 1S6, Canada  
e-mail: dallen@sfu.ca  
Tel.: +788-782-3967  
Fax: +788-782-4198

M. Journeay  
Geological Survey of Canada,  
Natural Resources Canada,  
101–605 Robson Street, Vancouver, BC V0N 1G0, Canada

**Resumen** Se calibró y validó un enfoque de ámbito hidroestructural en acuíferos de macizo rocoso fracturado de las Islas del Golfo, Columbia Británica (CB), Canadá. Se derivaron propiedades hidráulicas potenciales relativas para tres ámbitos hidroestructurales en rocas sedimentarias falladas y plegadas usando datos de fracturas generados estocásticamente y un modelizado de medio poroso equivalente de red de fracturas discretas híbridas (MPE-RFD). Los valores de transmisividad potenciales relativos

derivados del modelo muestran buena congruencia espacial con valores de transmisividad obtenidos de pruebas de bombeo en sitios seleccionados. Un patrón espacial de transmisividad ascendente hacia el suroriente a lo largo de la cadena de islas es consistente entre ambos grupos de datos. El análisis de aglomerados de los valores de permeabilidad potencial relativa obtenidos del conjunto más grande de datos para la región identificó cuatro aglomerados con medias geométricas de  $9 \times 10^{-13}$ ,  $4 \times 10^{-13}$ ,  $2 \times 10^{-13}$ , y  $3 \times 10^{-14} \text{ m}^2$ . La tendencia general es un incremento permeabilidad potencial relativa hacia el sureste, emulando las tendencias identificadas en los análisis específicos para los sitios. Los valores de permeabilidad potencial relativa incrementan con la proximidad relativa a la línea de la charnela de una estructura regional con pliegues de propagación y falla asimétrica de orientación noroeste y con la cercanía a fallas frágiles superpuestas de alto ángulo de orientación nor-noreste. Los resultados son consistentes con patrones documentados de flujo de fluidos controlados estructuralmente y son prometedores para usarlos en caracterización regional de acuíferos de macizo rocoso fracturado.

**Keywords** Heterogeneity · Fractured rocks · Hydraulic properties · Tectonics · Canada

## Introduction

Structural features such as folds, faults and fracture networks, have the potential to significantly influence

regional-scale fluid flow. As a result, hydraulic properties derived from site-scale investigations may not provide an accurate representation of bulk properties when extrapolated to a regional scale. Characterizing the permeability at a regional scale where fracture distributions are heterogeneous, can be aided by defining hydrostructural domains. Such an approach uses regional-scale structural data to divide aquifers into structural domains (Ohlmacher 1999; Martin and Tannant 2004), which are delineated by changes in the geometry, orientation or distribution of fold and fault structures and associated fabric elements, with the premise that each domain is characterized by a unique set of hydraulic properties. The term ‘hydrostructural domain’, which has not been widely adopted within the literature is, in some respects, synonymous with ‘structural domains’, but has the explicit connotation of affecting the hydraulic properties of aquifers. The term ‘hydrostratigraphic unit’ is similarly used to represent differences in the hydraulic properties in porous (sedimentary) rocks. At a regional scale, defining hydrostructural domains on the basis of relative-fracture network permeability offers a means of characterizing aquifers at a regional scale where fracture distributions are heterogeneous (e.g., Turkey Creek Watershed, Colorado, Caine and Tomusiak 2003; Äspö Hard Rock Laboratory, Sweden, Winberg et al. 2003). The use of a hydrostructural domain approach should result, therefore, in more accurate characterization and quantification of regional groundwater resources for fractured rock aquifers.

Mackie (2002) used bedrock geology and mesoscopic structural features to divide the Gulf Islands, British

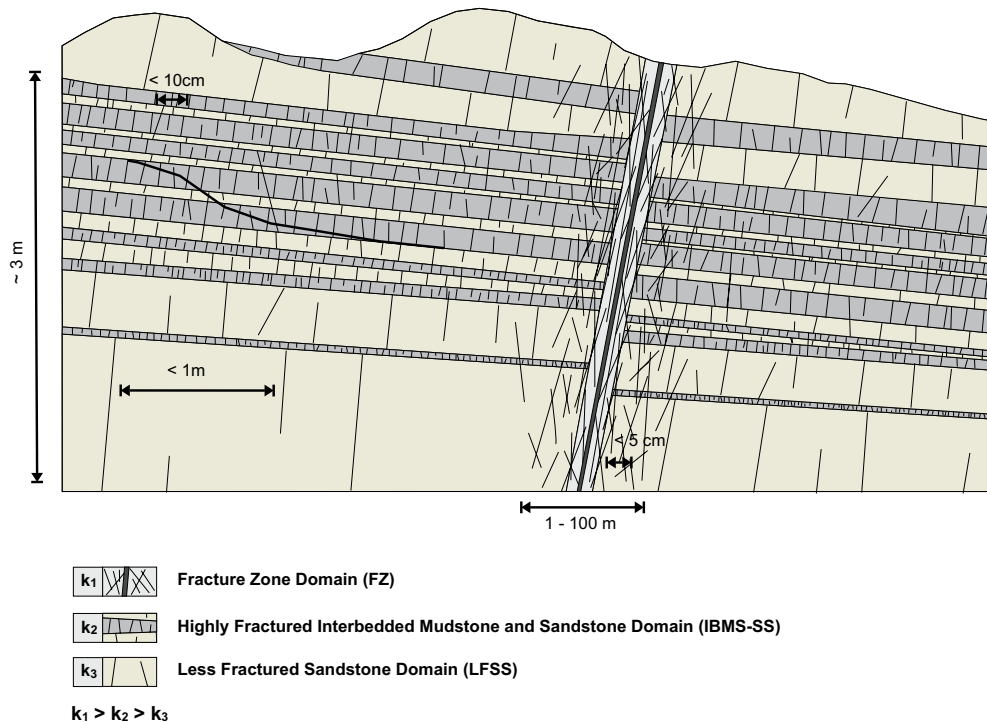


**Fig. 1** Hydrostructural domain conceptual model for the southern Gulf Islands showing in order of decreasing relative potential permeability ( $k$ ): *fault and fracture zone domain (FZ)*, *highly fractured interbedded mudstone and sandstone domain (IBMS-SS)*, and *less fractured sandstone dominant domain (LFSS)*. Estimated fracture spacing for each domain is shown as well as typical dimensions at the outcrop scale. Figure not to scale (modified from Denny et al. 2007)

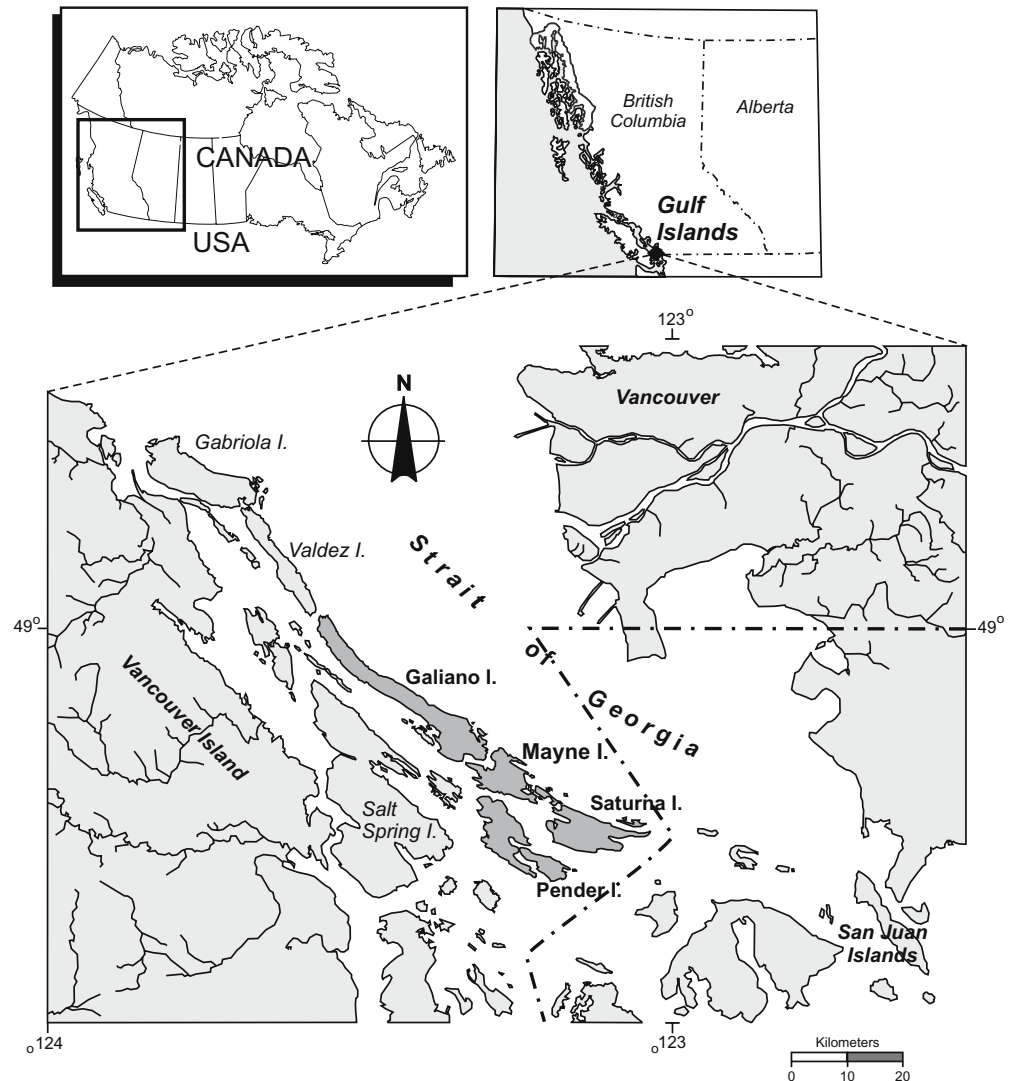
Columbia, Canada into three hydraulically distinct hydrostructural domains. These domains are, in part, lithology-dependent and reflect changes in fracture intensity within the rock mass. They include: ‘highly’ fractured interbedded mudstone and sandstone (IBMS-SS) with fracture spacing <10 cm and an average fracture intensity of 8.0, ‘less’ fractured sandstone (LFSS) with fracture spacing >1 m and average fracture intensity of 1.0, and fault and fracture zones (FZ) with fracture spacing of <5 cm and average fracture intensities of 9.0 (Fig. 1). Fracture intensity is defined as the number of fractures per unit scanline length ( $L^{-1}$ ). The fracture measurements indicate that permeability likely increases closer to fault and fracture zones and within the highly fractured interbedded mudstone and sandstone domain.

Previous work on Mayne Island, one of the four southern Gulf Islands, demonstrated that a hydrostructural domain model approach can be used to characterize the bulk hydraulic properties of the fractured rock aquifer at a small scale (Surette and Allen 2007). In that work, the potential porosity and relative potential permeability for

the island were estimated using a hybrid discrete fracture network-equivalent porous medium (DFN-EPM) modeling approach. The model results showed that the most permeable units on Mayne Island were the IBMS-SS and FZ hydrostructural domains with relative potential permeabilities on the order of  $10^{-13} \text{ m}^2$ . This value is an order of magnitude greater than the value of  $10^{-14} \text{ m}^2$  obtained for the LFSS domain. These results suggest that the IBMS-SS domains are likely the dominant water transmitting aquifers on Mayne Island, a conclusion supported by drilling and geophysical observations (Allen et al. 2002). However, although these rock units are pervasive throughout the Gulf Islands, the estimates obtained using the DFN-EPM model for Mayne Island may not necessarily be representative of the regional nature of bulk hydraulic parameters throughout the Gulf Islands.

In this paper, a hydrostructural domain approach is used to characterize and quantify the regional nature of bulk hydraulic parameters for Galiano, Mayne, Pender and Saturna Islands, all members of the Gulf Islands (Fig. 2). The aim of the study is to test whether or not the

**Fig. 2** Location map and regional setting of the southern Gulf Islands in this study



hydrostructural domain approach implemented on Mayne Island can be equally applied across the Gulf Islands region, and to determine whether any regional trends in the hydraulic properties can be related to the regional scale structure. To do this, the hydraulic properties of each domain, specifically relative potential transmissivity and permeability, were derived using stochastically generated fracture data and DFN-EPM modelling. The heterogeneity of the fractured rock is interpreted within the context of the defined hydrostructural domains, and the bulk hydraulic properties for each island are estimated. Model-derived relative potential transmissivity values are compared to estimates of transmissivity from pumping tests at selected sites. The pattern of relative potential transmissivity and permeability across the four islands are then identified using cluster analysis. These patterns enable an assessment of the relationship between large-scale structural features and bulk hydraulic properties in the Gulf Islands.

## Regional context

The Gulf Islands are located within the Strait of Georgia on the southwest coast of British Columbia. The study focuses on four of the southernmost outer Gulf Islands: Saturna Island, Pender Island, Mayne Island and Galiano Island (Fig. 2). The islands range in area from approximately 20 to 60 km<sup>2</sup> with elevations up to 400 m above sea level. The topography of the islands is controlled primarily by NW–SE trending ridges and valleys.

Regional scale groundwater characterization is important in the Gulf Islands, as groundwater is generally the sole source of potable water for domestic and agricultural use in a region with very low recharge rates and fractured, low-yielding bedrock aquifers. Groundwater is derived primarily from the fractured sedimentary rocks of the Late Cretaceous Nanaimo Group (~91–66 Ma). The Nanaimo Group is divided into eleven formations, which comprise mainly alternating sequences of interbedded sandstone-dominant and mudstone (or siltstone)-dominant formations

(Table 1). The contacts between the formations are typically transitional and are usually characterized by the presence of interbeds. While massive sandstone units are common, massive mudstone units are not; mudstone is typically interbedded with sandstone. The primary porosity of the Nanaimo Group is low and is considered to be of minor importance in the storage and transport of groundwater (Dakin et al. 1983; England 1990). As a result, permeability is thought to be derived primarily from fractures.

Four major tectonic features are present in the sedimentary rocks of the Nanaimo Group and these provide the secondary porosity necessary for groundwater movement. From oldest to youngest, these structural features include: (1) northwest trending, northeast dipping thrust faults associated with compression by a southwest vergent thrust system (England and Calon 1991; Mustard 1994; Journeay and Morrison 1999), (2) northwest-trending buckle folds and associated northeast-vergent thrust faults resulting from southeast-directed extension (Journeay and Morrison 1999), (3) shallow dipping features representing bedding plane partings, which are suggested to have formed during uplift and/or isostatic rebound after deglaciation (Mackie 2002) and, (4) northeast trending fault and fracture zones as well as bedding perpendicular jointing, which are present at a local scale (Mustard 1994; Mackie 2002).

The hydrostructural domains defined by Mackie (2002) were defined on the basis of fracture intensity measured in the sandstone (LFSS), the interbedded mudstone and sandstone (IBMS-SS), and in association with faults and fracture zones (FZ) as illustrated in Fig. 1.

## Methods

### Pumping test data

A total of 29 pumping tests were selected from a previous study to obtain field-based transmissivity values for the aquifers on three of the southern Gulf Islands (Allen et al. 2003). Only well sites in close spatial proximity to fracture data collection sites were selected to provide a

**Table 1** Lithofacies descriptions of the Nanaimo Group strata examined in this study (geological descriptions summarized from Mustard 1994) and hydrostructural domain designations

Formation	Description	Hydrostructural domain
Extension	Clast-supported, moderately to poorly sorted pebble to cobble conglomerate, with medium coarse-grained lithic arenite matrix. Sandstone interbeds present and increase in upper section of formation	LFSS
Pender Protection	Massive to thin-bedded mudstone and siltstone with interbeds of finely grained sandstone	IBMS-SS
Cedar District	Primarily medium- to thick-bedded sandstone with interbeds or siltstone	LFSS
de Courcy	Thin bedded silty shale, siltstone and fine grained sandstone which commonly contain carbonate concretions	IBMS-SS
Northumberland	Thick bedded, medium to very coarse sandstone with fine-grained sandstone, siltstone and mudstone interbeds.	LFSS
Geoffrey	Silty shale with thin interbeds of very fine-grained sandstone and siltstone; minor thick-bedded medium- to coarse-grained sandstone	IBMS-SS
Spray	Thick bedded, medium- to coarse-grained sandstone, pebble to cobble conglomerate; prominent interbeds of shale	LFSS
Gabriola	Mudstone and siltstone sequences with varying amounts of sandstone interbeds	IBMS-SS
	Thick bedded, coarse- to medium-grained arkosic sandstone with rare laminated silty mudstone interbeds	LFSS

reasonable comparison between field-based and simulated aquifer properties. The 29 well sites are situated on three of the four Gulf Islands in this study; the majority of the sites (22 sites) are located on Galiano Island (Fig. 3). Pumping test data were not available for Pender Island. Twenty-seven of the pumping tests were conducted in wells completed in the sandstone-dominant LFSS domain, and only two were completed in the mudstone-dominant IBMS-SS domain. Many of the wells tested had been drilled close to fracture zones within the LFSS in an effort to increase well yield. As a result, there may be a bias in the pumping test data towards the LFSS domain as well as potentially inflated hydraulic properties relating to fracture zones.

Hydraulic data obtained from the pumping tests were analyzed and reported by Allen et al. (2003) using the derivative method to identify periods of radial flow

(Bourdet et al. 1984; Allen 1999). Transmissivity values, calculated from both the pumping and recovery data using the Theis and Theis Recovery Methods (Theis 1935; Kruseman and de Ridder 1994), yielded consistent values of transmissivity. Therefore, only the transmissivity values calculated from the pumping period data were used for this study.

### Fracture data

Using Mackie's (2002) conceptual model for the southern Gulf Islands, representative exposures for each hydrostructural domain present in the study area were selected through field reconnaissance. A total of 87 outcrops comprise the composite dataset (Fig. 3). Fracture orientation, intensity, aperture and trace length were sampled

**Fig. 3** Simplified geologic maps for **a** Galiano Island, **b**, Mayne Island, **c** Saturna Island, and **d** Pender Island showing the sandstone dominant (LFSS) and mudstone dominant (IBMS-SS) hydrostructural domains of the Nanaimo Group. Fracture data collection sites are shown (2004–2005 signifies fracture data collected for this study (e.g., G7-8); fracture data collected in a previous study are denoted as 2002 and identified with an asterisk, e.g., 148\*) with corresponding equal-area projections of poles to fractures ( $n$  number of measurements; contour interval is  $2\sigma$ ). Water well sites used for pumping test analysis are also shown. No pumping test data were available for Pender Island

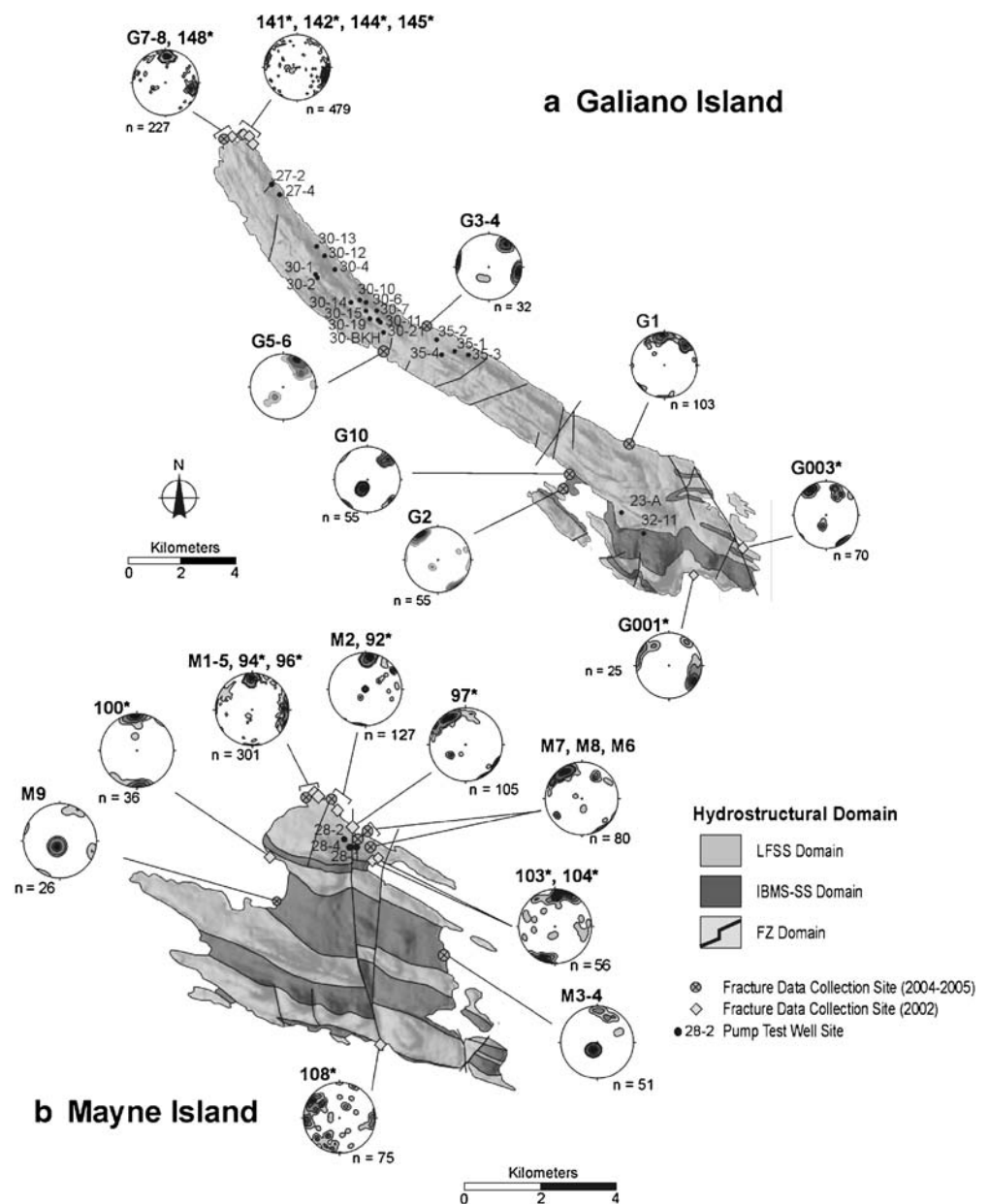
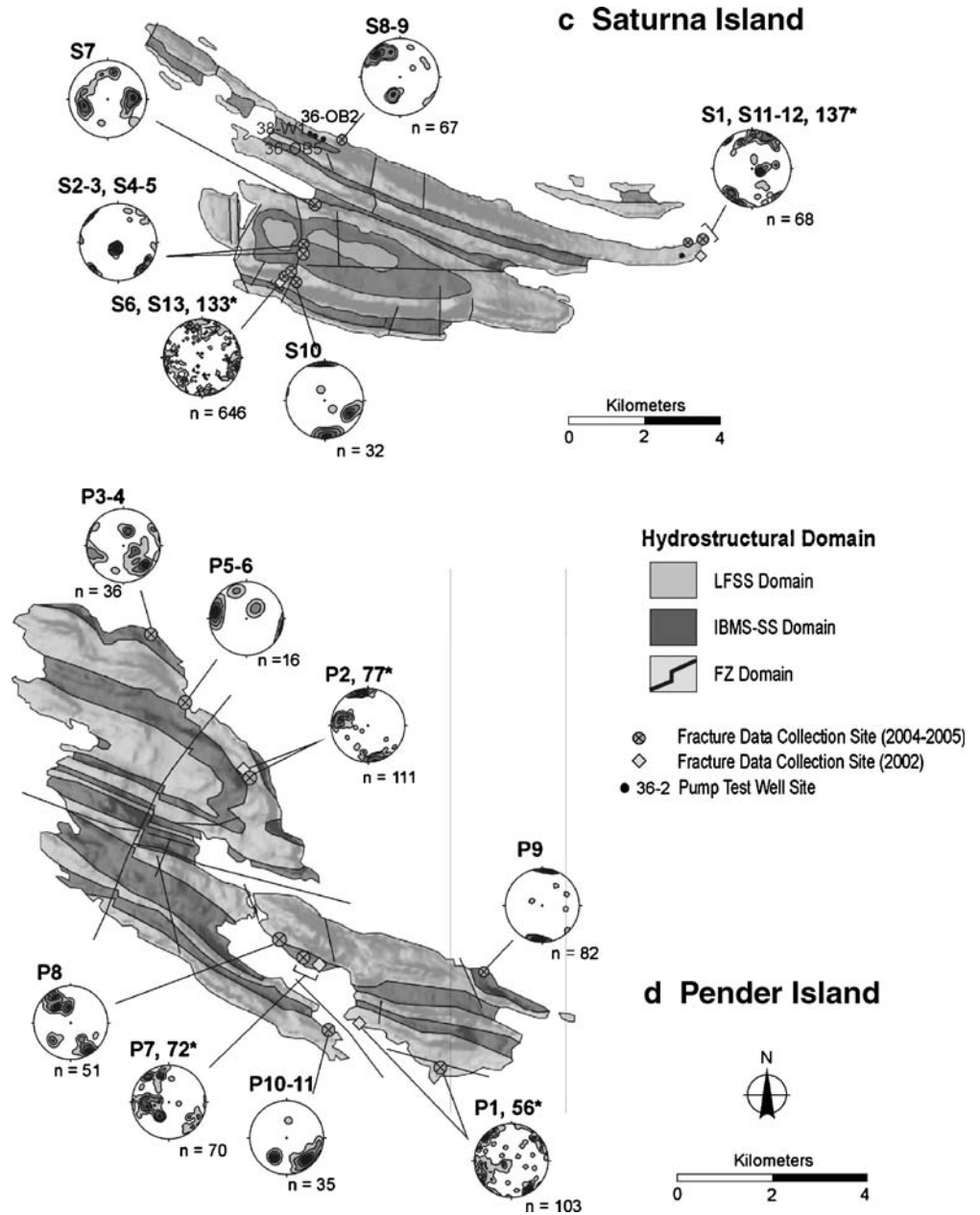
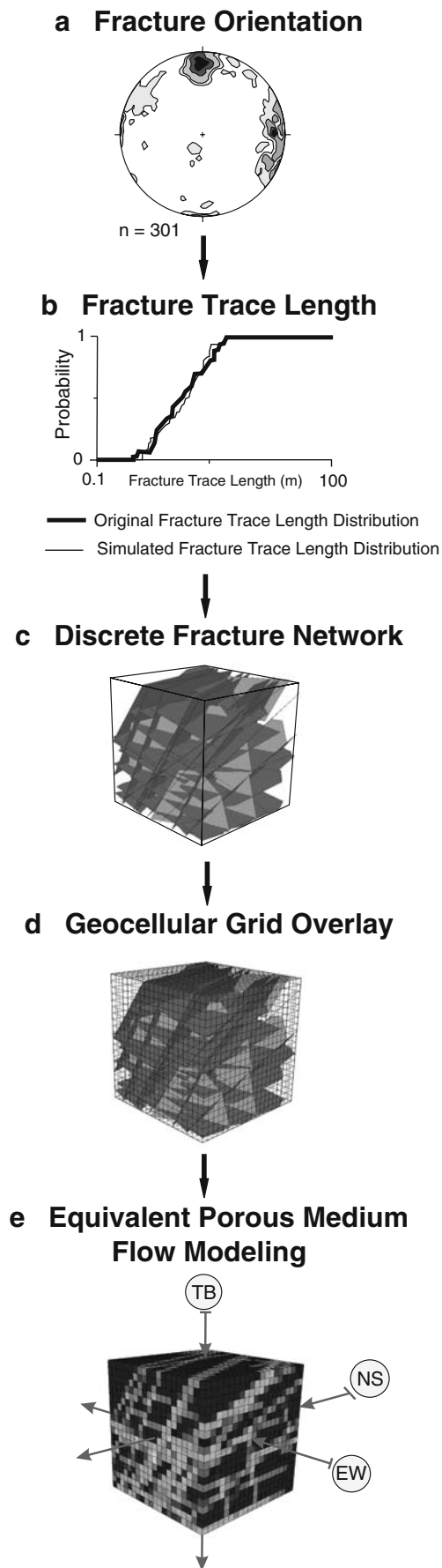


Fig. 3 (continued)



using a scanline technique. In this technique, a graduated tape measure is stretched across an outcrop face at near right angles to major fracture sets to avoid scanline orientation bias (Caine and Tomusiak 2003). Orientation bias can result in complete sub-horizontal fracture sets being missed in the sampling. In this study, exposures with at least two near-orthogonal faces were targeted to capture fractures that were sub-parallel to one of the outcrop faces. This method further reduces scanline orientation bias as fractures sub-parallel to one face will be recorded on the second face (Terzaghi 1965; Baecher 1983). The average scanline length was 30 m, but many were considerably smaller, particularly in the finer grained materials.

Drill core data were not available for this study. Although drill cores provide a solution to measuring subsurface fracture sets, logistical restraints often result in surface fracture expression being the only viable option for estimating subsurface densities (e.g., Caine and Tomusiak 2003; Neuman 2005). Thus, fracture measurements taken at the surface were used as a proxy for the subsurface. In adopting this proxy it is recognized that fracture sets measured on outcrop surfaces do not completely characterize their distribution in three dimensions, especially in the subsurface (Mauldon et al. 2001). Fractures that appeared to be closed at the surface (due to mineralization or simply because they had no observable aperture) were measured, but were not included in the analysis.



◀ **Fig. 4** Flowchart outlining the DFN-EPM modeling process. Best-fit probability density functions are determined for fracture orientation data (a), as well as for the fracture trace length estimates (b). Fracture sets are simulated within a DFN model domain (c). An EPM grid is applied to the DFN model (d). Flow is applied according to a simple geographic coordinate system (e). *NS* north-south; *EW* east-west; *TB* top to bottom

A Watson-Williams' test-of-means for spherical data was conducted on the composite dataset to compare fracture orientation measurements from the three hydrostructural domains in order to determine equivalency of fracture orientation within each domain, and to distinguish the different domains. The method, as proposed by Mardia (1972), converts azimuth and dip fracture measurements to polar coordinates for the calculation of a resultant vector. The resultant length of that vector is a measure of the concentration around a mean direction, if one exists. The calculated resultant lengths are used in an F-approximation to test if the mean fracture orientations of the two data sets are statistically different or not (Mardia 1972). The null hypothesis for the F-test states that the mean directions from two samples are not significantly different, and this hypothesis is rejected when the calculated F-statistic is greater than the critical value for a desired level of significance. Critical values at the 95% confidence interval were obtained from significance tables published by Fisher et al. (1987). Using this confidence interval, the Watson-Williams' test-of-means results showed that fractures within the same hydrostructural domain tend to have similar fracture orientation, and that these orientations are statistically different from those in other hydrostructural domains on the same island. An interesting finding is that, while the hydrostructural domains had originally been defined based on fracture intensity, the statistics suggest that fracture orientation can also be used to distinguish between domains.

### Model construction

The FracSys module of the FracMan package was used for a statistical analysis of the fracture data (Dershowitz et al. 1998). A workflow for the modeling process is shown in Fig. 4. The FracSys algorithm, encompassing a series of sub-algorithms, uses a forward modeling approach to determine the statistical distributions for fracture orientation and trace length that are a 'best-fit' of the field data (Dershowitz 1995).

For fracture orientation, an algorithm assigns fracture data to sets and determines the probability density functions that best describe those sets. The premise is that the sets should be groups of fractures with similar properties (Dershowitz et al. 1996). Fracture sets can be distinguished by a number of parameters including orientation, mineralization species, relative ages, length and morphology (Caine and Tomusiak 2003). In this study, fracture orientation was the sole parameter used for set designation. Weighting factors of other fracture

characteristics such as mineralization, were set to zero. A soft sector convergence method was specified, which increases the probability of the assignment of fractures to sets with mean poles in the same sector. A sector is defined by the midpoint between set mean pole vectors (Dershowitz et al. 1998).

An initial approximation of the orientation distribution that best describes each fracture set, and the mean direction and dispersion factors for each of the distributions were defined in terms of a mean pole vector estimated through parametric analysis using SpheriStat (Pangaea Scientific 1998). The initial guess of the best-fit probability density function for each fracture set was determined through visual inspection of the symmetry of the fracture data on equal area Schmidt nets and also a trial and error approach. Five types of probability distributions for directional data are possible: the univariate and bivariate Fisher distribution, the bivariate normal distribution, the bivariate Bingham distribution, and the spherical Dirac delta constant distribution.

The distribution of properties for the fractures assigned to each set is calculated, and then fractures are re-assigned to sets according to probabilistic weights proportional to their similarity to other fractures in the set. The properties of the sets are then recalculated, and the process repeated iteratively until the set assignment is optimized. Optimization is achieved when the goodness-of-fit between the measured and simulated field observations is statistically

significant using two-sample Kolmogorov-Smirnov (K-S) test. A K-S test determines whether two underlying one-dimensional probability distributions differ, or whether an underlying probability distribution differs from a hypothesized distribution, in either case based on finite samples. The two-sample K-S test is one of the most useful and general nonparametric methods for comparing two samples, as it is sensitive to differences in both location and shape of the empirical cumulative distribution functions of the two samples. A statistical significance of 0.1 (90% confidence) was sought, although not always achieved, as some data were difficult to fit to such a high significance level. The results indicate that fracture set orientations are typically best-fit with Fisher (Fisher 1953; Davis 2002) and Bivariate Bingham (Dershowitz et al. 1998) probability distribution functions. K-S test results range from 32.5 to 100%, with an average of 80.2%.

For fracture length, an algorithm is used to determine the distribution of fracture radii that gives the best match to the fracture trace length data collected in the field. The sampling process is simulated by recording fracture sizes encountered within a specified survey window size; window size is defined by the scanline length multiplied by the transverse length (Dershowitz et al. 1998). The method accounts for fracture censoring, truncation and sampling bias by using a simulated sampling method, and similar to the orientation algorithm, requires an assumed distribution of the fracture

**Table 2** Transmissivity values derived from the analysis of pumping test data using the Theis method (after Allen et al. 2003)

Islands <sup>a</sup>	Well ID	Well type	Domain	Well depth (m)	Length of open hole (m)	Theis-T (m <sup>2</sup> /s) <sup>b</sup>
Saturna	36-W1	P	LFSS	19.0	17.0	6.45 × 10 <sup>-5</sup>
	36-OB2	O	LFSS	30.5	24.4	4.80 × 10 <sup>-5</sup>
	36-OB5	O	LFSS	48.8	42.7	7.19 × 10 <sup>-5</sup>
Mayne	38-DW	P	LFSS	106.7	100.6	1.48 × 10 <sup>-5</sup>
	28-1	P	LFSS	134.1	131.1	1.17 × 10 <sup>-5</sup>
	28-2	P	LFSS	30.5	25.0	2.49 × 10 <sup>-5</sup>
Galiano	28-4	P	LFSS	103.6	101.2	2.49 × 10 <sup>-5</sup>
	23-A	P	IBMS-SS	54.9	48.3	2.02 × 10 <sup>-5</sup>
	27-2	P	LFSS	38.1	32.0	1.79 × 10 <sup>-6</sup>
	27-4	P	LFSS	61.9	60.6	7.65 × 10 <sup>-7</sup>
	30A-1	P	LFSS	118.9	118.6	3.05 × 10 <sup>-6</sup>
	30A-2	O	LFSS	131.1	130.5	2.57 × 10 <sup>-6</sup>
	30A-4	P	LFSS	61.0	44.5	2.98 × 10 <sup>-6</sup>
	30A-6	P	LFSS	121.9	117.3	1.09 × 10 <sup>-6</sup>
	30A-7	P	LFSS	83.8	83.2	2.82 × 10 <sup>-6</sup>
	30A-10	P	LFSS	54.9	48.5	1.56 × 10 <sup>-6</sup>
	30A-11	P	LFSS	45.7	45.7	2.72 × 10 <sup>-6</sup>
	30A-12	P	LFSS	45.7	43.0	2.05 × 10 <sup>-5</sup>
	30A-13	P	LFSS	108.2	104.5	3.98 × 10 <sup>-7</sup>
	30A-14	P	LFSS	167.6	164.6	1.99 × 10 <sup>-6</sup>
	30A-15	P	LFSS	45.7	42.1	1.71 × 10 <sup>-5</sup>
30B-19	P	LFSS	45.7	45.4	2.09 × 10 <sup>-5</sup>	
30B-21	P	LFSS	99.1	97.8	1.63 × 10 <sup>-6</sup>	
30B-BKH	P	LFSS	30.8	30.2	1.95 × 10 <sup>-5</sup>	
32-11	P	IBMS-SS	83.8	77.7	3.61 × 10 <sup>-5</sup>	
35-1	P	LFSS	85.3	85.3	4.32 × 10 <sup>-5</sup>	
35-2	P	LFSS	121.9	121.9	3.38 × 10 <sup>-7</sup>	
35-3	P	LFSS	36.6	36.6	3.34 × 10 <sup>-5</sup>	
35-4	P	LFSS	54.9	54.9	1.79 × 10 <sup>-5</sup>	

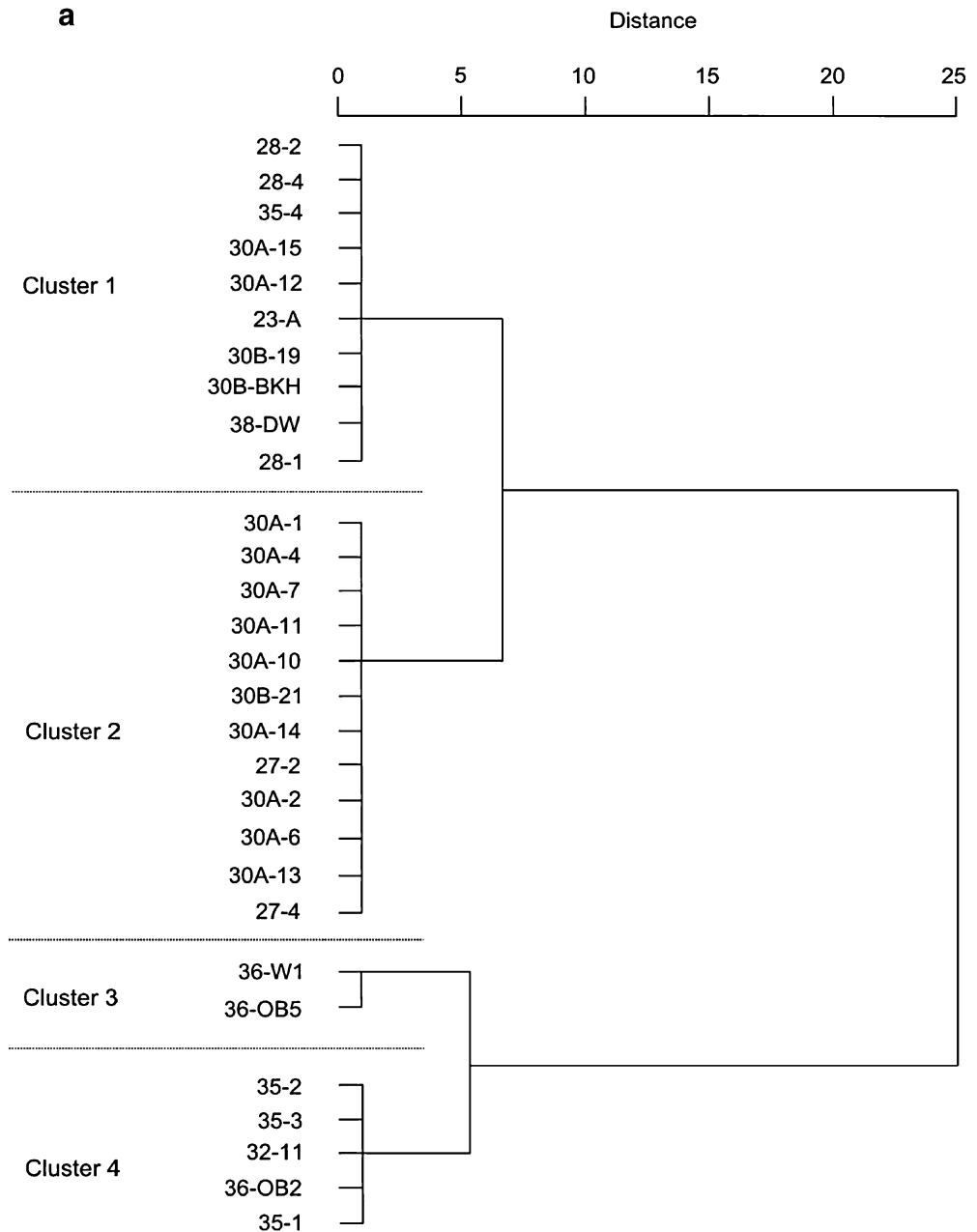
<sup>a</sup> Pumping test data were not available for Pender Island.

<sup>b</sup> Theis-T is the estimated transmissivity using the Theis method of analysis for pumping tests.

Well type: *P* pumping well, *O* observation well. Well locations shown on Fig. 3



**Fig. 5** Cluster analysis dendrograms showing the division of the clustered data into three clusters **a** pumping test transmissivity, **b** potential transmissivity, and **c** potential permeability. Statistically, the values in each cluster are similar

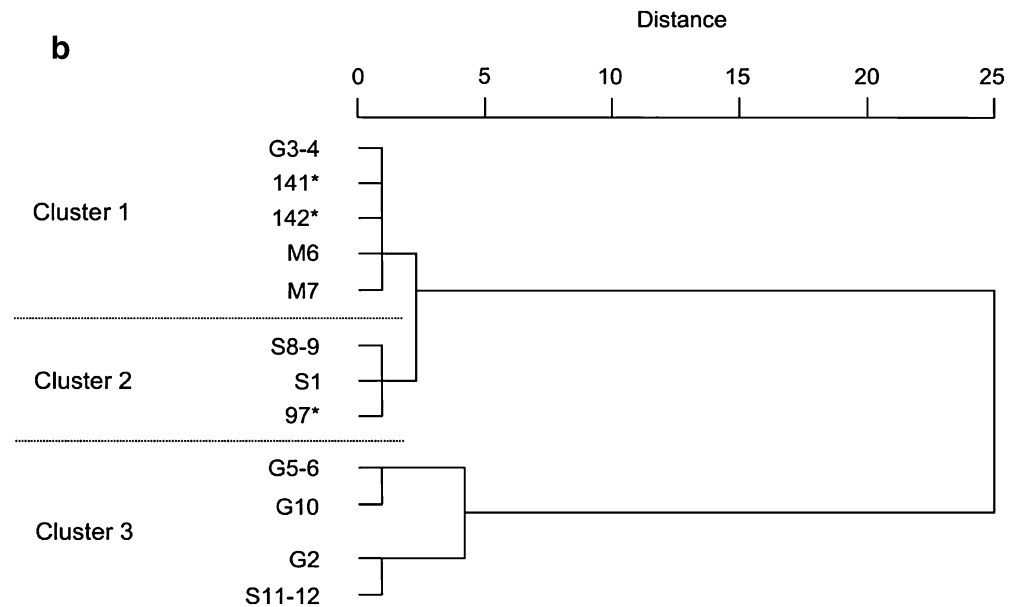


radii to begin the simulation process. The probability distributions for scalar data supported by the algorithm are the uniform, exponential, power law, normal, lognormal, gamma and Dirac delta constant distributions. An automated search for the best-fit match between the simulated sample distribution and the actual data is done using a simulated annealing optimization algorithm (Dershowitz et al. 1998), which generates five realizations of the assumed distribution for each iteration in an effort to improve the match between the simulated and observed distributions. The simulations are repeated until a satisfactory match is obtained, as determined by the K-S statistic. Similar to above, a statistical significance of 0.1 was considered acceptable. The majority of the fracture trace length data are log-normally distributed; however,

some of the data are better approximated by exponential, power law and constant distributions. K-S test results range from 51.7% to 100% with an average of 84.1%.

Discrete fracture network (DFN) models were constructed for each fracture data collection site on the four islands using FracWorks XP (Golder Associates Inc. 2004). Each DFN model domain was constructed as a  $20 \times 20 \times 20$ -m cube, and populated with fractures according to the orientation and trace length probability distributions (Fig. 4). The model domain size was determined based largely on computational efficiency, as solutions could not be obtained for larger domains in the more densely fractured materials. For most of the sites, the domain size corresponds with the scanline mapping scale, and likely approximates the representative elementary

Fig. 5 (continued)



volume (REV). However, for some simulations, a  $100 \times 100 \times 100$ -m cube would have been ideally used based on maximum fracture lengths of about 50 m measured in some outcrops.

The DFN models were then calibrated to field fracture data using a simulated scanline within the model domain. The simulated scanline maintains the same orientation (trend/plunge) as the field, thereby removing the need to correct for fractures not perpendicular to the scanline, while maintaining the same fracture spacing distribution. During this process, the number of fractures per unit scanline length is first converted to volumetric fracture intensity, resulting in a fracture surface area per unit volume. A simulated scanline is then generated, and the fracture set intensity along the simulated scanline compared to field values. The modeled fracture set is regenerated until the simulated fracture intensity matches the observed fracture set intensity with a relative error less than 10%. Ultimately, the best-fit DFN model for each site was identified.

In conducting a DFN analysis, fracture network geometry and fracture transmissivity distribution are the key parameters (NRC 1996). A number of assumptions had to be made in respect of modelling parameters simply because insufficient data were available from the subsurface (i.e., core data and packer tests) to adequately define these parameters. This is a common limitation of outcrop-based studies. However, the values used were within the ranges used in other studies and provide a baseline for comparison of potential permeability values across the region.

The simulated fractures were modeled as smooth, parallel-walled, hexagonal fractures with no elongation (an aspect ratio of one). This simplification was required as fracture characteristics estimated at surface do not necessarily provide a good estimate of conditions at depth due to the effects of weathering. Fracture spacing was described by an enhanced Baecher model (Dershowitz et al. 1998) following a Poisson process, as field observa-

tions suggested that the fractures were randomly distributed with no clear tendency towards clustering. Fracture set termination percentages, calculated from field observations, were honoured statistically in the DFN models. A uniform fracture aperture of  $100 \mu\text{m}$  ( $0.0001 \text{ m}$ ) was assumed for all fractures in the model, even though applying a uniform fracture aperture is not thought to accurately represent natural fractures (Liu 2005; Neuman 2005). The value selected is nonetheless consistent with estimates of fracture aperture used in other outcrop-based studies (e.g., Caine and Tomusiak 2003). Furthermore, employing a uniform aperture eliminates one variable and facilitates a comparison of the hydrostructural domains based solely on orientation and fracture length data. In a sense, this provides a standardized approach.

Transmissivity values for individual fractures, typically acquired through packer testing, were not available for this study as domestic wells were inaccessible. Therefore, a constant transmissivity value of  $6.24 \times 10^{-7} \text{ m}^2/\text{s}$ , calculated using the cubic law (e.g., Snow 1968) using the assigned aperture, was assumed for all the fractures in the model.

The best-fit DFN model for each site was transformed into a  $0.2 \times 0.2 \times 0.2$ -m MODFLOW grid (1 million grid cells) that contains cell-specific hydraulic properties calculated using the Oda Analysis process (Fig. 4) (Oda 1985). Grid spacing was selected as a compromise between a reasonable grid refinement and processing capacity. The MODFLOW platform GMS (EMRL 2005) was then used for the continuum modeling. A custom code was written to transform the FracMan output file into a format that GMS recognizes.

Surette and Allen (2007) tested the significance of the two assumptions expected to most likely influence the results (i.e., fracture aperture and EPM grid size) using a factorial analysis approach fashioned after Starzec and Andersson (2002). They show that the chosen fracture aperture and equivalent porous medium-grid-spacing end

Fig. 5 (continued)

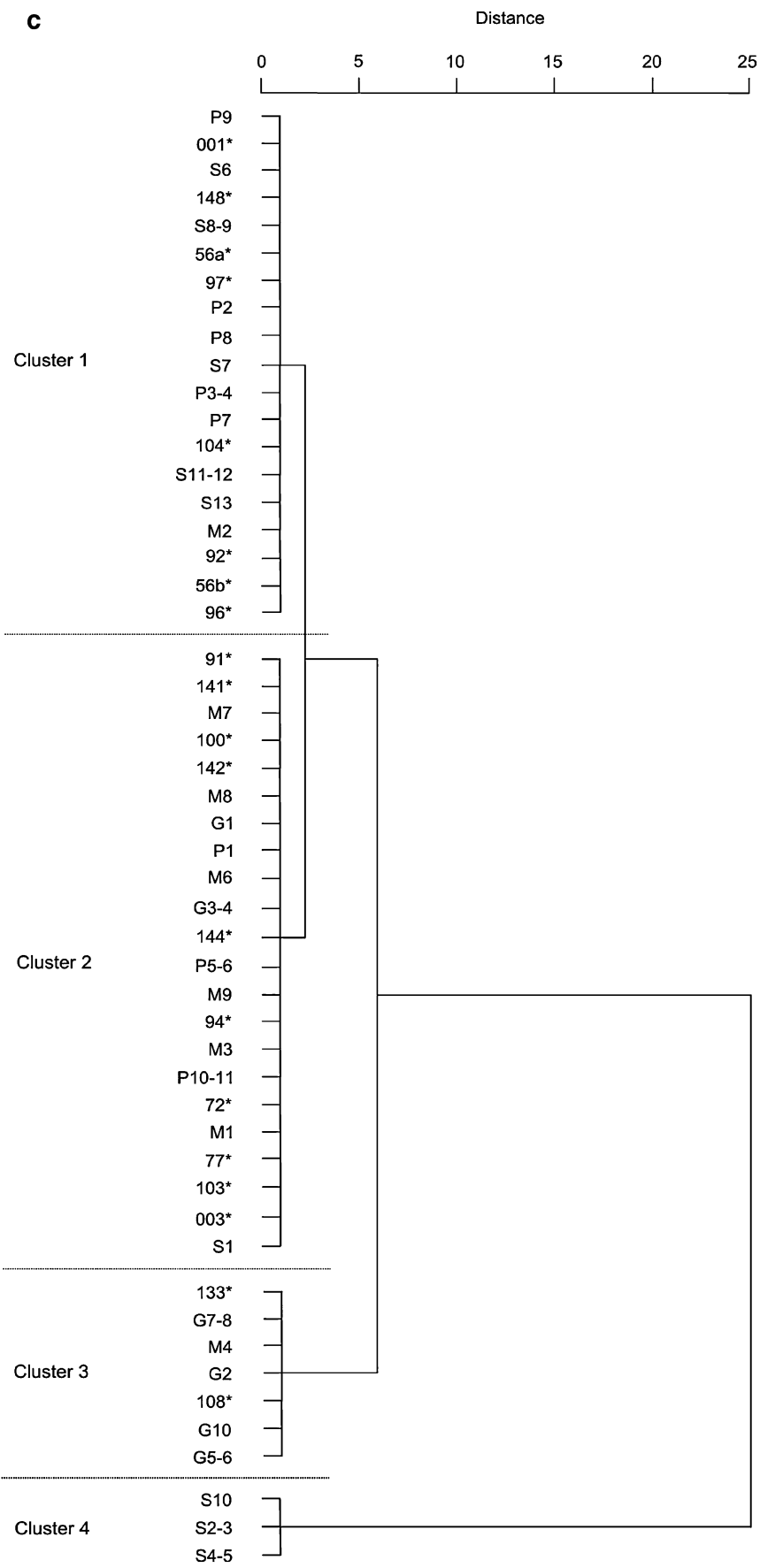
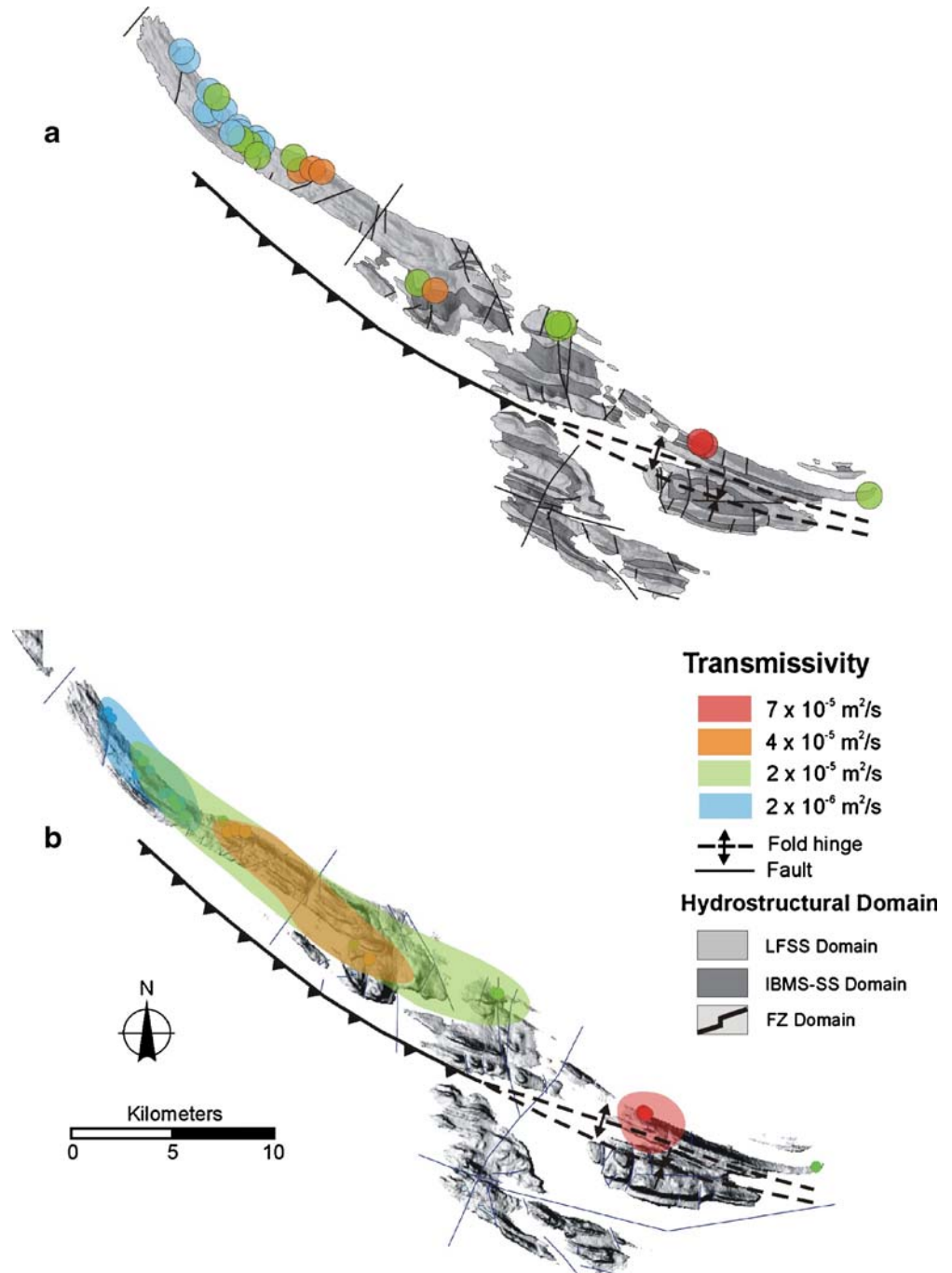


**Table 3** Cluster analysis results for the pumping test transmissivity values

Geometric mean			
Pumping test transmissivity, $T$ ( $m^2/s$ )			
Cluster 1	Cluster 2	Cluster 3	Cluster 4
$7 \times 10^{-5}$	$4 \times 10^{-5}$	$2 \times 10^{-5}$	$2 \times 10^{-6}$

members, as well as their interactions, do not significantly affect the difference between relative potential permeability of the model used and the sensitivity analysis models (representing variations in fracture aperture and grid size).

**Fig. 6** Spatial distribution of the clustered field-based transmissivity data with **a** clustered data points in relation to hydrostructural domains, and **b** clustered data points highlighted to show spatial pattern overlain on shaded relief map



Thus, the relative potential permeability estimates, obtained using the model variables, provide reasonably accurate approximations.

### Parameter estimation

Estimates of relative potential fracture network permeability require flow simulations through the fracture networks. To do this, steady-state flow was simulated between two opposing faces of the hybrid discrete fracture network-equivalent porous medium (DFN-EPM) model. Boundary conditions were assigned according to a simple

**Table 4** Model simulated potential transmissivity results

Islands	Scanline ID	Domain	Well ID	Open hole length b (m)	Model hydraulic conductivity $K$ (m/s)	Model transmissivity $T$ (m <sup>2</sup> /s)	Geometric mean transmissivity $T$ (m <sup>2</sup> /s)
Saturna	S8-9	LFSS	36-W1	17.0	$1.32 \times 10^{-6}$	$2.25 \times 10^{-5}$	$3.45 \times 10^{-5}$
			36-OB2	24.4		$3.23 \times 10^{-5}$	
			36-OB5	42.7		$5.65 \times 10^{-5}$	
Mayne	S1 S11-12 M6	LFSS	38-DW	100.6	$3.01 \times 10^{-7}$	$3.03 \times 10^{-5}$	$3.03 \times 10^{-5}$
			38-DW	100.6		$9.43 \times 10^{-5}$	
			28-1	131.1		$1.59 \times 10^{-5}$	
Mayne	M7	LFSS	28-2	25.0	$1.98 \times 10^{-7}$	$3.03 \times 10^{-6}$	$1.37 \times 10^{-5}$
			28-4	101.2		$1.23 \times 10^{-5}$	
			28-1	131.1		$2.60 \times 10^{-5}$	
Mayne	97 <sup>a</sup>	FZ	28-2	25.0	$1.09 \times 10^{-6}$	$4.95 \times 10^{-6}$	$7.58 \times 10^{-5}$
			28-4	101.2		$2.01 \times 10^{-5}$	
			28-1	131.1		$1.43 \times 10^{-4}$	
Galiano	G3-4	LFSS	28-2	25.0	$1.32 \times 10^{-7}$	$2.74 \times 10^{-5}$	$8.88 \times 10^{-6}$
			28-4	101.2		$1.11 \times 10^{-4}$	
			35-1	85.3		$1.12 \times 10^{-5}$	
Galiano	G5-6	FZ	35-2	121.9	$3.51 \times 10^{-6}$	$1.60 \times 10^{-5}$	$1.74 \times 10^{-4}$
			35-3	36.6		$4.81 \times 10^{-6}$	
			35-4	54.9		$7.22 \times 10^{-6}$	
Galiano	141 <sup>a</sup>	LFSS	30A-11	45.7	$1.77 \times 10^{-7}$	$1.60 \times 10^{-4}$	$7.78 \times 10^{-6}$
			30B-19	45.4		$1.59 \times 10^{-4}$	
			30B-21	97.8		$3.43 \times 10^{-4}$	
Galiano	142 <sup>a</sup>	LFSS	30B-BKH	30.2	$2.10 \times 10^{-7}$	$1.06 \times 10^{-4}$	$9.28 \times 10^{-6}$
			27-2	32.0		$5.65 \times 10^{-6}$	
			27-4	60.6		$1.07 \times 10^{-5}$	
Galiano	G2	IBMS-SS	27-2	32.0	$2.24 \times 10^{-6}$	$6.73 \times 10^{-6}$	$1.13 \times 10^{-4}$
			27-4	60.6		$1.28 \times 10^{-5}$	
			23-A	48.3		$1.08 \times 10^{-4}$	
Galiano	G10	IBMS-SS	23-B	53.1	$3.14 \times 10^{-6}$	$1.19 \times 10^{-4}$	$1.59 \times 10^{-4}$
			23-A	48.3		$1.51 \times 10^{-4}$	
			23-B	53.1		$1.67 \times 10^{-4}$	

<sup>a</sup> Designates fracture data collected previously by Mackie (2002).

geographic coordinate system after Caine and Tomusiak (2003). An arbitrary, uniform hydraulic head gradient of 0.01 m/m was applied to the model using specified head boundaries at opposing cube faces in each of the principal geographic directions (Fig. 4). Zero flux conditions were specified on the remaining four model faces. This approach results in three flow simulations for each model (N–S, E–W, and top to bottom). In conducting flow simulations in this fashion, an attempt is made to standardize the flow field so as to determine if there are relative differences in the potential permeability between the different domains, and identify any trends that might exist at the regional scale. Any differences in relative potential permeability will accentuate the variability in fracture orientation (hence the term ‘relative’) throughout the region. To determine the actual permeability tensor would require construction of a flow field for an infinite number of directions. This problem was tackled for one island in the study area (Surrette and Allen 2007).

**Table 5** Cluster analysis results for the model-derived potential transmissivity values

Geometric mean		
Potential transmissivity, $T_p$ (m <sup>2</sup> /s)		
Cluster 1 $1 \times 10^{-4}$	Cluster 2 $4 \times 10^{-5}$	Cluster 3 $9 \times 10^{-6}$

The volumetric fluid flux is computed along each specified head boundary, and then used to calculate the equivalent bulk potential permeability for each model domain in each direction using Darcy’s Law:

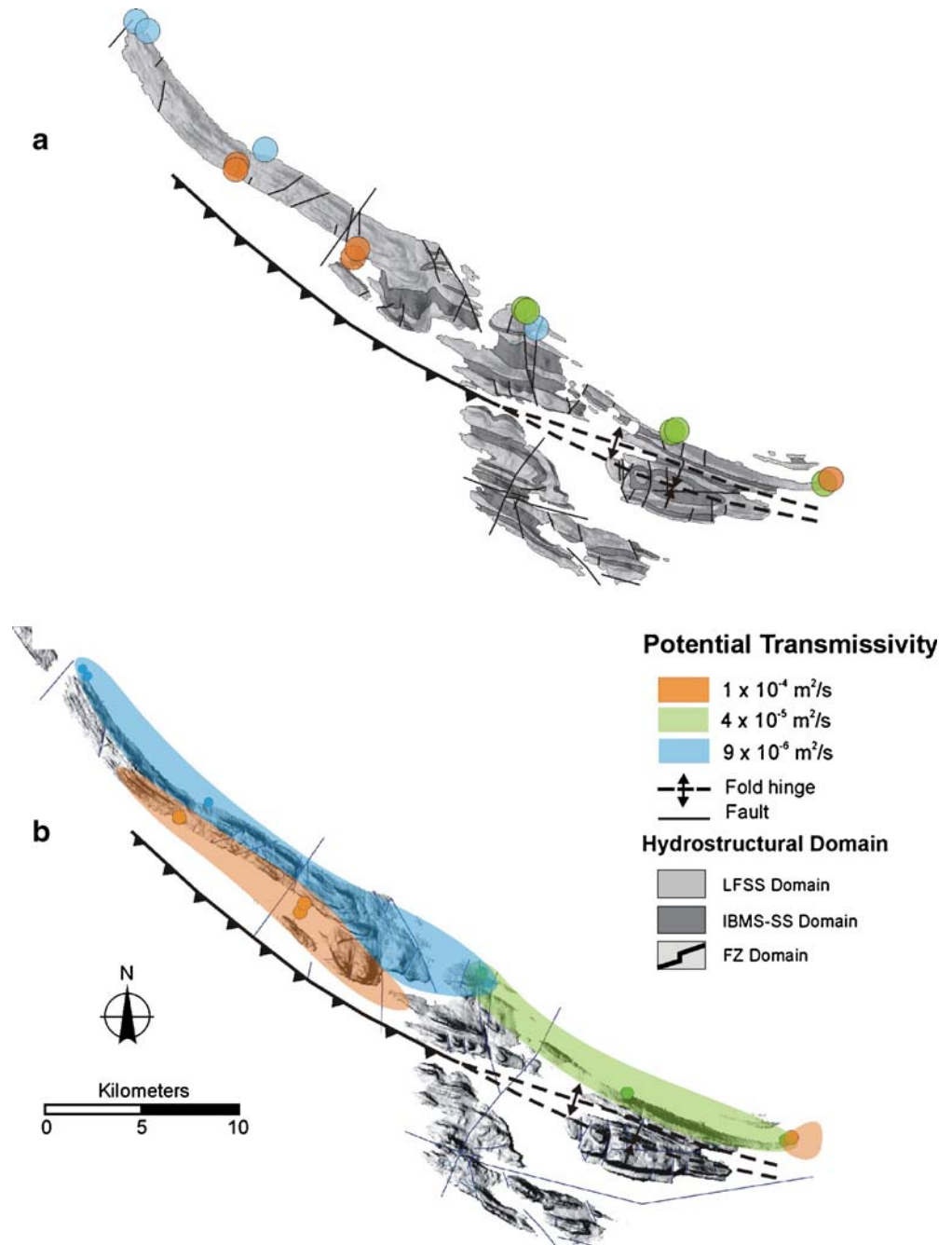
$$k_p = \frac{\mu}{\rho g} \frac{Q}{IA} \quad (1)$$

where  $Q$  is the simulated volumetric flow rate (L<sup>3</sup>/T),  $I$  is a specified hydraulic gradient (dimensionless),  $A$  is a specified cross sectional area (L<sup>2</sup>) across which  $Q$  flows,  $\rho$  is fluid density (M/L<sup>3</sup>),  $g$  is the acceleration due to gravity (L/T<sup>2</sup>), and  $\mu$  is the dynamic fluid viscosity (M/LT). In this study, the values of relative potential permeability are dependent on the aperture and transmissivity distributions assigned to each fracture in the DFN model, and were not constrained by site-specific hydraulic data.

The estimation of relative potential transmissivity for DFN-EPM models situated close to hydraulic test well sites allows for a comparison between field-based and model-simulated transmissivity values. Potential transmissivity is estimated from hydraulic conductivity ( $K$ ), which is related to potential permeability (Eq. 1) obtained from the DFN-EPM model results:

$$K = k_p \left( \frac{\rho g}{\mu} \right) \quad (2)$$

**Fig. 7** Spatial distribution of the clustered model-derived potential transmissivity data with **a** clustered data points in relation to hydrostructural domains, and **b** clustered data points *highlighted* to show spatial pattern overlain on shaded relief map



where  $k_p$  is the simulated potential permeability ( $L^2$ ),  $\rho$  is fluid density ( $M/L^3$ ),  $g$  is the acceleration due to gravity ( $L/T^2$ ), and  $\mu$  is the dynamic fluid viscosity ( $M/LT$ ) (Fetter 1994). The calculated hydraulic conductivity is, in turn, used to estimate the model potential transmissivity ( $T_p$ ):

$$T_p = Kb \quad (3)$$

where  $K$  is the hydraulic conductivity calculated from the hybrid DFN-EPM model ( $L/T$ ) and  $b$  is the saturated thickness of the aquifer ( $L$ ). The value of  $b$  for bedrock aquifers is assumed to be equal to the length of the open

interval (i.e., the depth of the well minus the depth of casing). For this study, the open interval of a well nearest to a model site was used in the calculation of potential transmissivity for that model.

### Cluster analysis

Cluster analysis (CA) is a classification method that is used to arrange a set of observations within a population into homogeneous 'like' groups (Davis 2002). The aim of CA is to minimize differences between observations within a cluster and maximize differences between

**Table 6** Summary of potential permeability results for the hybrid DFN-EPM models

Islands	Domain	Domain geometric mean $k_p$ (m <sup>2</sup> )
Saturna	LFSS	$9.6 \times 10^{-14}$
	FZ	$3.8 \times 10^{-13}$
Pender	LFSS	$9.0 \times 10^{-14}$
	IBMS-SS	$2.5 \times 10^{-13}$
Mayne	FZ	$1.5 \times 10^{-13}$
	LFSS	$4.3 \times 10^{-14}$
	IBMS-SS	$1.1 \times 10^{-13}$
Galiano	FZ	$1.2 \times 10^{-13}$
	LFSS	$2.2 \times 10^{-14}$
	IBMS-SS	$3.5 \times 10^{-13}$
	FZ	$2.6 \times 10^{-13}$

Detailed results are provided in the [Electronic supplementary material](#).

observations contained in other clusters. Hierarchical CA achieves this by defining a distance measure (similarity measure) between every pair of data points. A squared Euclidean distance measure of similarity is used in this study, which gives the straight-line distance between two observations:

$$d_{x,y} = \sum_{i=1}^n (x_i - y_i)^2 \quad (4)$$

where  $d_{x,y}$  is the sum of the squared distances between object  $x$  and object  $y$ . A large distance signifies dissimilarity between two observations. In agglomerative hierarchical CA, each observation is initially considered as a separate cluster. Two observations with the smallest distance measured and, thus, the highest similarity are combined, and the distance is recalculated. This process is reiterated until all observations have been agglomerated into a cluster.

Ward's method (Ward 1963) was used in this study. This agglomerative hierarchical method determines the order of clustering of groups containing more than one observation. Ward's method iteratively joins two clusters that minimize the sum of squares within a cluster, while maximizing the sum of squares between clusters. The sum of squares within a cluster is defined as:

$$SS_k = \sum (x_{ik} - \bar{x}_k)^2 \quad (5)$$

where  $SS_k$  is the sum of squares within a cluster  $k$ ,  $\bar{x}_k$  is the centroid of a cluster  $k$ , and  $x_{ik}$  is an individual object within the cluster (Davis 2002). The sum of squares between clusters 1 and 2 is:

$$SS_{1,2} = \sum (\bar{x}_1 - \bar{x}_2)^2 \quad (6)$$

As a result, Ward's clustering joins clusters that maximize between-group variability, while keeping the with-in group variability to a minimum. The relative

distances between the clusters are displayed on a dendrogram plot where the number of 'like' groups is visually identified by breaks in the dendrogram.

Cluster analysis was used in this study to provide a less subjective way of separating model results (e.g., relative potential permeability) into relatively homogeneous sub-groups. Following clustering of the model data, breaks in the dendrograms were visually identified and the number of 'like' clusters determined. The spatial distributions of the 'like' clusters were then mapped in ArcGIS 8.0.

## Results and discussion

### Pumping test data

The pumping test analysis results show that measured transmissivity values vary spatially throughout the Gulf Islands. Maximum values were obtained on Saturna Island and minimum values on southeast Galiano Island (Table 2). The transmissivity values from four well sites located on the southeast and northwest ends of Saturna Island within the LFSS domain range from  $7.2 \times 10^{-5}$  to  $1.5 \times 10^{-5}$  m<sup>2</sup>/s with a geometric mean of  $4.3 \times 10^{-5}$  m<sup>2</sup>/s. The transmissivity values from three pumping tests conducted on northwest Mayne Island within the LFSS domain range from  $2.5 \times 10^{-5}$  to  $1.2 \times 10^{-5}$  m<sup>2</sup>/s with a geometric mean of  $1.9 \times 10^{-5}$  m<sup>2</sup>/s. On Galiano Island, twenty wells are completed in the sandstone-dominant LFSS domain and have transmissivity values ranging from  $4.3 \times 10^{-5}$  to  $3.4 \times 10^{-7}$  m<sup>2</sup>/s with a geometric mean of  $3.9 \times 10^{-6}$  m<sup>2</sup>/s. Only two pumping tests were available within the mudstone-dominant IBMS-SS domain at the southeast end of Galiano Island. Transmissivity values were  $3.6 \times 10^{-5}$  and  $2.0 \times 10^{-5}$  m<sup>2</sup>/s with a geometric mean of  $2.7 \times 10^{-5}$  m<sup>2</sup>/s.

To better interpret the pumping test transmissivity results, a cluster analysis (CA) was conducted. Four clusters were identified (Fig. 5a). The range in transmissivity is not significant, with geometric mean values ranging from  $2 \times 10^{-6}$  to  $7 \times 10^{-5}$  m<sup>2</sup>/s (Table 3). Mapping the transmissivity values identified in each cluster suggests a weak spatial trend of increasing transmissivity to the southeast from Galiano Island to Saturna Island (Fig. 6). Deviations from this relationship are interpreted to be the consequence of elevated transmissivity resulting from localized second-order fracture zones and geologic contacts. These high values are derived from pumping tests conducted in domestic and sub-division wells that were drilled preferentially close to fracture zones in an effort to increase well yield. For example, well sites on mid-Galiano Island have relatively 'high' transmissivity associated with a mapped

**Table 7** Cluster analysis results for the potential permeability values

Geometric mean			
Potential permeability, $k_p$ (m <sup>2</sup> )			
Cluster 1	Cluster 2	Cluster 3	Cluster 4
$9 \times 10^{-13}$	$4 \times 10^{-13}$	$2 \times 10^{-13}$	$3 \times 10^{-14}$

**Fig. 8** Graphs showing changes in model permeability for each of the geographic coordinate flow directions **a** N-S, **b** E-W, and **c** top to bottom, with respect to the topographically driven groundwater flow angle relative to north

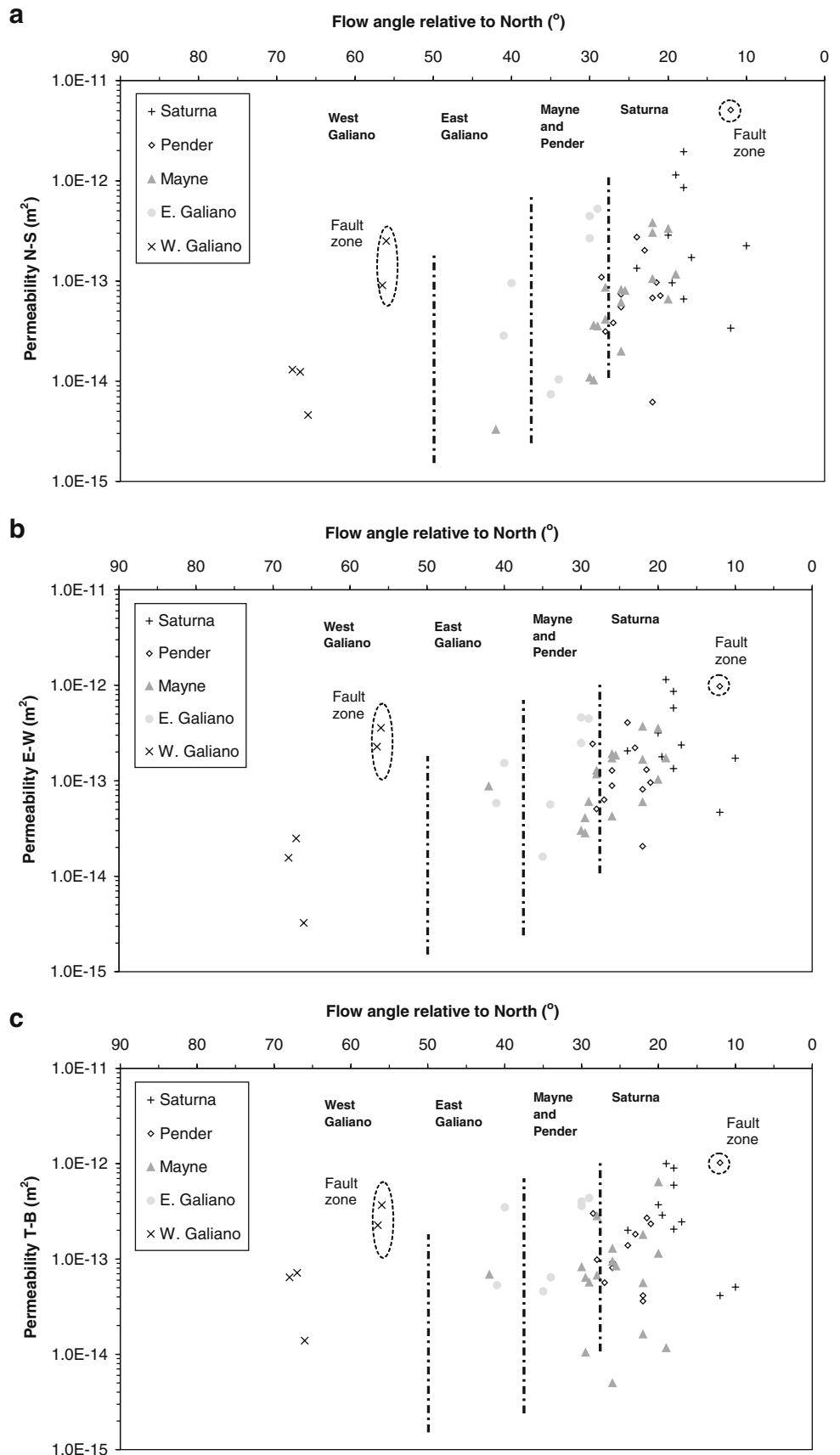
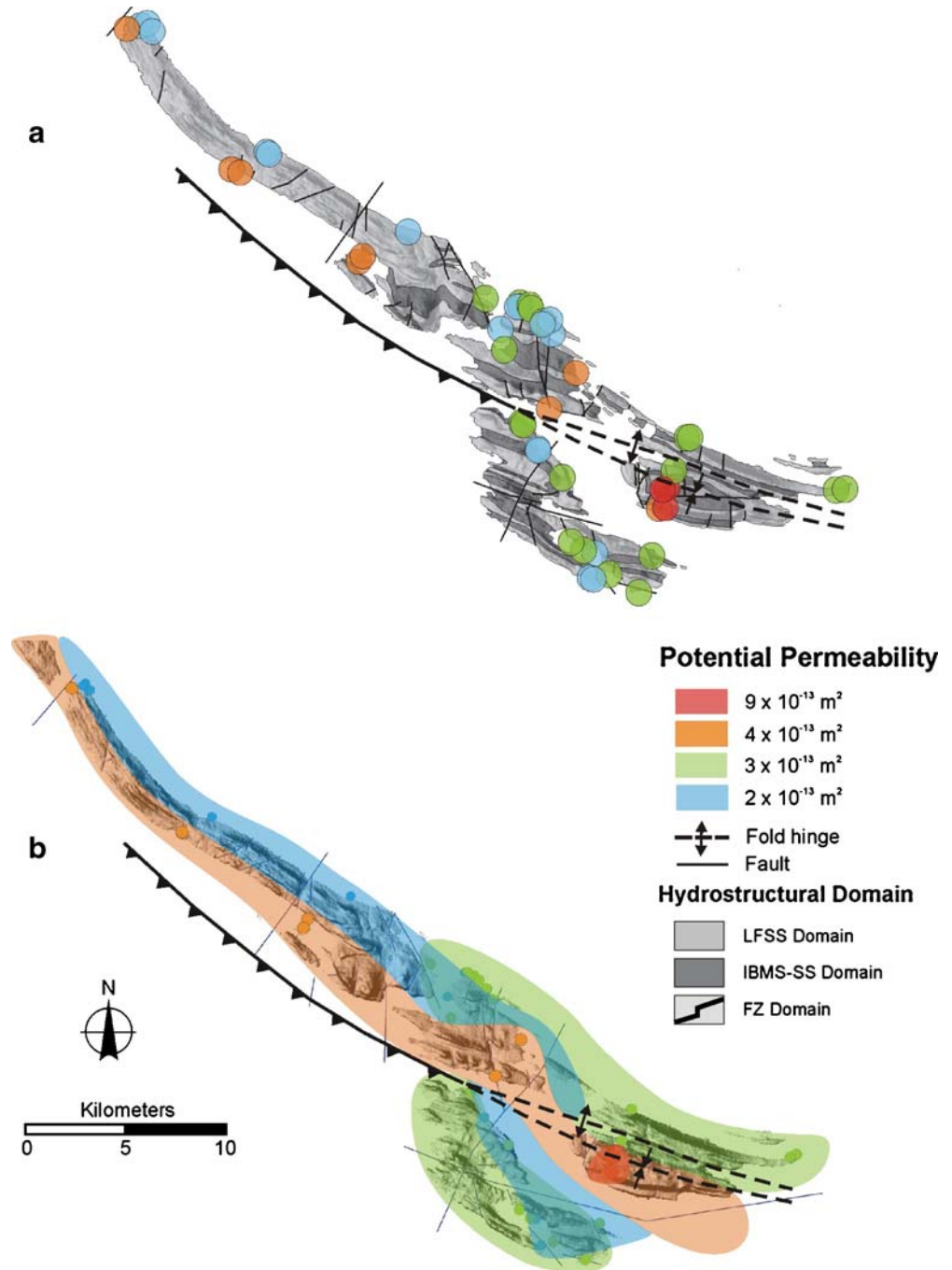




**Fig. 9** Spatial distribution of the clustered potential permeability data with **a** clustered data points in relation to hydrostructural domains; and **b** clustered data points *highlighted* to show spatial pattern overlain on shaded relief map



northeast trending fault zone (Fig. 6). Because of this drilling bias, some of the measured transmissivity results are inflated. As a result, not only do the values shed ambiguity on the regional trend, but they may not be representative of the LFSS domain overall.

The occurrence of elevated transmissivity within fault zones is consistent with the regional stress model proposed for the Gulf Islands by Journey and Morrison (1999), which suggests that northeast trending faults lie within a zone of extension. Consequently, these fractures likely have open apertures and, therefore, increased measured transmissivity. In fact, higher well yields are

commonly reported to occur in the vicinity of these northwest-trending structures, hence the targeted drilling into fracture zones.

### **Potential transmissivity**

Estimates of relative potential transmissivity calculated from 12 DFN-EPM models situated close to pumping test well sites range from  $7.78 \times 10^{-6}$  to  $1.74 \times 10^{-4} \text{ m}^2/\text{s}$  (Table 4). The relative potential transmissivity values estimated from the three model sites on the southeast and northwest ends of Saturna Island (LFSS domain) gave a geometric mean of  $4.6 \times$

$10^{-5}$  m<sup>2</sup>/s. The two models situated within the LFSS domain on northwest Mayne Island yielded a geometric mean transmissivity value of  $1.1 \times 10^{-5}$  m<sup>2</sup>/s, and a single model within the FZ domain, also on northwest Mayne Island, gave a geometric mean transmissivity of  $7.58 \times 10^{-5}$  m<sup>2</sup>/s. On Galiano Island, the three models situated in the LFSS domain yielded a geometric mean transmissivity of  $8.6 \times 10^{-6}$  m<sup>2</sup>/s. A geometric mean transmissivity of  $1.3 \times 10^{-4}$  m<sup>2</sup>/s was calculated for the two models located in the IBMS-SS domain on southeast Galiano, and  $1.74 \times 10^{-4}$  m<sup>2</sup>/s for a model in the FZ domain, also on southeast Galiano. The general trend of the estimated model transmissivity values is an average increase in transmissivity from northwest to southeast, emulating the subtle trend identified from pumping test analysis.

A cluster analysis on the DFN-EPM modeled data also identifies a pattern of southeastward increasing relative potential transmissivity values (Fig. 5b). The analysis identified three clusters with geometric mean transmissivity values of  $1 \times 10^{-4}$ ,  $4 \times 10^{-5}$  and  $9 \times 10^{-6}$  m<sup>2</sup>/s, respectively (Table 5). Although a map of the spatial distribution of these values is not well defined, the underlying trend does reflect the pumping test results and also shows a subtle pattern of increasing transmissivity to the southeast along the chain of islands (Fig. 7). Of the 12 model sites for which relative potential transmissivity estimates were obtained, two are located within the FZ domain and two within the IBMS-SS domain on Galiano Island (Fig. 7). Therefore, the DFN-EPM simulated relative potential transmissivity values are likely biased towards these highly fractured domains. Despite these biases, the similarity in magnitude and spatial distribution of the measured aquifer transmissivities indicates that the DFN-EPM models are representative of the aquifers of the southern Gulf Islands at a regional scale.

### Potential permeability

Due to the low number of sites used to estimate relative potential transmissivity from DFN models (12 situated near sites where pumping tests were conducted), the entire Gulf Islands fracture database was analyzed to provide a more comprehensive view of the results.

Estimates of relative potential permeability throughout the Gulf Islands indicate an overall increase in value to the southeast from Galiano Island to Saturna Island (see Table 8 in [Supplementary electronic material](#)). The permeability of the LFSS domain increases to the southeast of Galiano Island, with domain geometric means increasing from  $2.2 \times 10^{-14}$  to  $9.6 \times 10^{-14}$  m<sup>2</sup> (Table 6). The distribution and degree of permeability within the IBMS-SS and FZ domains are comparable, and show an increasing trend in permeability from Mayne Island to Saturna Island. The permeability of the IBMS-SS domain increases from  $1.1 \times 10^{-13}$  m<sup>2</sup> on Mayne Island to  $2.5 \times 10^{-13}$  m<sup>2</sup> on Pender Island (Table 6). The mudstone-dominant sites on Saturna Island were not included in the IBMS-SS analysis as the Saturna sites are in close proximity to a major fault zone and, therefore, were included within the FZ domain. The FZ domain potential

permeability also increases to the southeast from  $1.2 \times 10^{-13}$  to  $3.8 \times 10^{-13}$  m<sup>2</sup> along the axis of the island chain (Table 6).

Cluster analysis on all of the relative potential permeability estimates identified four clusters (Fig. 5c). The four clusters range in potential permeability from  $3 \times 10^{-14}$  to  $9 \times 10^{-13}$  m<sup>2</sup> (Table 7). The spatial pattern of the potential permeability clusters is better defined compared to that of potential transmissivity simply due to the larger database used in the analysis.

The southeastward increase in the magnitude of relative potential permeability is interpreted to be synchronous with an increase in island scale fracturing. This pattern is likely related to the greater proportion of the IBMS-SS hydrostructural domain on Saturna Island relative to the dominance of the LFSS domain on northwest Galiano Island. It is further suggested that the increase may be partially controlled by structures that are more aligned in the extensional domain of regional crustal stresses along the active plate margin, possibly resulting in open and/or wider fracture apertures. As indicated earlier, fractures that appeared to be closed at the surface (either due to mineralization or simply because they had no observable aperture) were not included in the analysis. Thus, increases in relative potential permeability should reflect the greater percentage of open fractures included in the models.

Potential fracture network porosity ( $n$ ) was also calculated directly from the DFN model results as the ratio of the fracture void volume obtained by the model. It is a measure of the volume of fracture void space per unit volume of rock for the simulated geometric fracture network (Caine and Tomasiak 2003). Potential porosity provides a measure of the amount of groundwater storage that is potentially available within the fracture network. Unlike relative potential permeability, potential porosity does not require flow simulations through the discrete fracture networks. As a result, potential porosity is not influenced by artificially high values that can be the result of model flow direction paralleling the mean fracture orientation (i.e., N-S, E-W and top to bottom).

The simulated values of potential porosity for the Gulf Islands range over three orders of magnitude; from 0.004 to 0.2% for an assumed fracture aperture of 100  $\mu$ m (see Table 8 in [Supplementary electronic material](#)). Similar to the spatial pattern identified from the pumping test and model-derived transmissivity data, the island scale mean potential porosity of the LFSS domain decreases toward the southeast, from 0.01% on Galiano Island to 0.03% on Saturna Island. Both the IBMS-SS and FZ domains also show the same trend as the LFSS domain, with values increasing from 0.04 to 0.06% and 0.04 to 0.13%, respectively.

Relative potential permeability estimates do not appear to be an artefact of the geographic coordinate flow directions used in this study (Fig. 8). However, fractures that are oriented parallel to a model-induced flow direction do show increased permeability in that direction. For example, the identified fault zone on Saturna Island (Fig. 8) trends approximately NE-SW and also shows the greatest permeability in this direction. Although the

relative magnitude of permeability changes slightly between the three flow directions, the same general relationship remains the same.

Measured and modelled values of potential permeability appear to increase with proximity to the hinge-line of a regional fault propagation fold, and with proximity to a younger system of north and northeast-trending high-angle brittle faults and associated fracture networks. The sub-linear zone of high permeability identified in the cluster analysis trends approximately NE–SW, along the axis of the fault propagation fold structure (see for example Fig. 9). As fracture densities are known to increase in the hinge zones of fold structures, (NRC 1996), it is reasonable to expect that the highest porosity and permeability would also be found here. As a result, the spatial patterns observed in this study suggest that the regional fracturing and stress regime associated with the folding may have had a significant influence on permeability values in the Gulf Islands. This influence can be seen in decreasing permeability values observed progressively down the limbs of the fold, away from the antiformal hinge zone (Fig. 9). More detailed fracture measurements are needed to confirm this relationship.

## Conclusions

Results of this study demonstrate that a hydrostructural domain approach can be useful for characterizing and quantifying regional scale relative potential transmissivity and permeability patterns using discrete fracture network-equivalent porous medium (DFN-EPM) modeling. Cluster analysis on the transmissivity values derived from pumping tests identified four clusters with geometric means of  $7 \times 10^{-5}$ ,  $4 \times 10^{-5}$ ,  $2 \times 10^{-5}$ , and  $2 \times 10^{-6}$  m<sup>2</sup>/s. Elevated transmissivity values are detected near localized second-order fracture zones and geologic contacts. Cluster analysis on model-derived relative potential transmissivity values, at the 12 sites where pumping tests had been conducted, identified three clusters with geometric mean transmissivity values of  $1 \times 10^{-4}$ ,  $4 \times 10^{-5}$ , and  $9 \times 10^{-6}$  m<sup>2</sup>/s. Overall, the model-derived potential transmissivity values compare well with the transmissivity values obtained from pumping tests. In both modelled and observed data, there is a weak, but consistent, pattern of increasing transmissivity towards the southeast along the chain of islands, from Galiano Island to Saturna Island.

Cluster analysis on relative potential permeability values obtained from a larger dataset for the region identified four clusters with geometric means of  $9 \times 10^{-13}$ ,  $4 \times 10^{-13}$ ,  $2 \times 10^{-13}$ , and  $3 \times 10^{-14}$  m<sup>2</sup>. The general trend is an increase in relative potential permeability toward the southeast, emulating the trends identified in the site-specific analyses. There is also a spatial correlation between increased model-derived relative potential permeability values and proximity to the hinge of a large-scale antiformal fault-propagation fold structure running parallel

to the islands and superimposed high-angle brittle fault structures. The similarity in hydraulic properties derived from direct field measurement and modeling serves to validate the hydrostructural domain approach to quantifying hydraulic properties. As a result, the method used in this paper may have applications to other areas where groundwater resources in fractured rock aquifers are of interest.

**Acknowledgements** This research was funded by the National Sciences Engineering and Research Council of Canada (NSERC). The authors would like to thank W. Dershowitz of Golder Associates Ltd. for the use of the FracWorks XP software. We also thank M. Toews for computing support and M. Holt for field assistance. Guidance from J.S. Caine of the US Geological Survey is also greatly appreciated.

## References

- Allen DM (1999) An assessment of the methodologies used for analyzing hydraulic test data from bedrock wells in British Columbia. Report for groundwater section, water management branch, British Columbia ministry of environment, lands and parks, Queen's Printer, Victoria, Victoria, BC, 91 pp
- Allen DM, Abbey DG, Mackie DC, Luzitano R, Cleary M (2002) Investigation of potential saltwater intrusion pathways in a fractured aquifer using an integrated geophysical, geological and geochemical approach. *J Environ Eng Geophys* 7:19–36
- Allen DM, Liteanu E, Bishop TW, Mackie DC (2003) Determining the hydraulic properties of fractured bedrock aquifers on the Gulf Islands, British Columbia. Report to Ministry of Water, Land and Air Protection, Victoria, BC, March 2003, 107 pp
- Baecher GB (1983) Statistical analysis of rock mass fracturing. *J Int Assoc Math Geol* 15:329–348
- Bourdet D, Alagoa A, Ayoub JA, Pirard YM (1984) New type curves aid in analysis of fissured zone well tests. *World Oil* April:111–124
- Caine JS, Tomusiak SRA (2003) Brittle structures and their role in controlling porosity and permeability in a complex Precambrian crystalline-rock aquifer system in the Colorado rocky mountain front range. *Geol Soc Am Bull* 115:1410–1424
- Dakin RA, Farvolden RN, Cherry JA, Fritz P (1983) Origin of dissolved solids in groundwaters of Mayne Island, British Columbia, Canada. *J Hydrol* 63:233–270
- Davis JC (2002) *Statistics and data analysis in geology*. Wiley, New York, 638 pp
- Denny SC, Allen DM, Journeay JM (2007) DRASTIC-Fm: a modified vulnerability mapping method for structurally controlled aquifers in the southern Gulf Islands, British Columbia, Canada. *Hydrogeol J* 15:483–493
- Dershowitz W (1995) Interpretation and synthesis of discrete fracture orientation, size, shape, spatial structure and hydrologic data by forwards modelling. In: Myer LR, Tsang CF, Cook NGW, Goodman RE (eds) *Proceedings of the Conference on Fractured and Jointed Rock Masses*, 3–5 June 1992, Lake Tahoe, CA, USA, pp 579–586
- Dershowitz W, Busse R, Uchida M (1996) A stochastic approach for fracture set definition. In: Aubertinet al. (eds) *Rock mechanics*, Balkema, Rotterdam, pp 1809–1813
- Dershowitz W, Lee G, Geler J, Foxford T, La Pointe P, Thomas A (1998) *FracMan: interactive discrete feature data analysis, geometric modeling, and exploration simulation, version 2.6*. User documentation, Golder Associates, Seattle, Washington
- EMRL (Environmental Modeling Research Laboratory) (2005) *GMS version 6.0*. Brigham Young University, Provo, UT, USA
- England TDJ (1990) *Late Cretaceous to Paleogene evolution of the Georgia basin, southwestern British Columbia*. PhD Thesis, Memorial University, St. John's, NFLD, Canada, 481 pp

- England TDJ, Calon TJ (1991) The Cowichan fold and thrust system, Vancouver Island, southwestern British Columbia. *Geol Soc Am Bull* 103:336–362
- Fetter CW (1994) *Applied hydrogeology*. Prentice Hall, New Jersey, 691 pp
- Fisher RA (1953) Dispersion on a sphere. *Proceedings of the Royal Society of Edinburgh*, no. A217, Royal Society of Edinburgh, Edinburgh, pp 295–305
- Fisher NI, Lewis T, Embleton BJJ (1987) *Statistical analysis of spherical data*. Cambridge University Press, Cambridge, 329 pp
- Golder Associates Inc. (2004) *FracWorks XP: discrete feature simulator, version 4.0*. User documentation, Golder Associates, Seattle, Washington, 85 pp
- Journey JM, Morrison J (1999) Field investigation of Cenozoic structures in the northern Cascadia forearc, southwestern British Columbia. *Current Research, Paper 99-1A*, Geological Survey of Canada, Ottawa, ON, pp 239–250
- Kruseman GP, de Ridder NA (1994) Analysis and evaluation of pumping test data. Publication no. 47, International Institute for Land Reclamation and Improvement, Wageningen, Germany, 377 pp
- Liu E (2005) Effects of fracture aperture and roughness on hydraulic and mechanical properties of rocks: implication of seismic characterization of fractured reservoirs. *J Geophys Eng* 2:38–47
- Mackie DM (2002) An integrated structural and hydrogeologic investigation of the fracture system in the upper Cretaceous Nanaimo Group, Southern Gulf Islands, British Columbia. MSc Thesis, Simon Fraser University, Burnaby, BC, Canada, 358 pp
- Mardia KV (1972) *Statistics of directional data*. Academic Press, London, 357 pp
- Martin MW, Tannant DD (2004) A technique for identifying structural domain boundaries at the EKATI diamond mine. *Eng Geol* 74:247–264
- Mauldon M, Dunne WM, Rohrbaugh MB Jr (2001) Circular scanlines and circular windows: new tools for characterizing the geometry of fracture traces. *J Struct Geol* 23:247–258
- Mustard PS (1994) The upper Cretaceous Nanaimo Group, Georgia Basin. In: Monger JWH (ed) *Geology and geological hazards of the Vancouver region, southwestern British Columbia*. Geological Surv Can Bull 481:27–95
- Neuman SP (2005) Trends, prospects and challenges in quantifying flow and transport through fractured rocks. *Hydrogeol J* 13:124–147
- NRC (National Research Council) (1996) *Rock fractures and fluid flow: contemporary understanding and applications*. National Academy Press, Washington, DC, 551 pp
- Oda M (1985) Permeability tensor for discontinuous rock masses. *Geotechnique* 35:483–495
- Ohlmacher GC (1999) Structural domains and their potential impact on recharge to intermontane-basin aquifers. *Environ Eng Geosci* 5:61–71
- Pangaea Scientific (1998) *Spheristat for Windows, version 2.2*. Brockville, ON, Canada
- Snow DT (1968) Rock fracture spacings, openings, and porosities. *Proceedings of the American Society of Civil Engineers. J Soil Mech Found Div ASCE* 94:73–91
- Starzec P, Andersson J (2002) Application of two-level factorial design to sensitivity analysis of keyblock statistics from fracture geometry. *Int J Rock Mech Min Sci* 39:243–255
- Surette M, Allen DM (2007) Quantifying heterogeneity in fractured sedimentary rock using a hydrostructural domain approach. *Geological Society of America Bulletin*, in press
- Terzaghi RD (1965) Sources of error in joint surveys. *Geotechnique* 15:287–304
- Theis CV (1935) The relation between the lowering of the piezometric surface and the rate and duration of discharge of a well using ground-water storage. *Trans Am Geophys Union* 16:519–524
- Ward JH Jr (1963) Hierarchical grouping to optimize an objective function. *J Am Stat Assoc* 58:236–244
- Winberg A, Andersson P, Byegård J, Poteri A, Cvetkovic V, Dershowitz W, Doe T, Hermanson J, Gómez-Hernández JJ, Hautojärvi A, Billaux D, Tullborg E-L, Holton D, Meier P, Medina A (2003) Synthesis of flow, transport and retention in the block scale. Final report of the TRUE Block Scale project, Report 4, SKB Technical Report TR-02-16, SKB, Stockholm, Sweden, 114 pp